In vivo evaluation of marine collagen sponge for wound healing in a rat model

Yuliya Kulikova[1]*, Vladimir Popov[2], Stanislav Sukhikh[1], Alena Shilova[3], Maria Dubrova[3], Lubov Dishluk[1], and Olga Babich[1]

ABSTRACT

Collagen exerts local wound-healing effects and is widely used in clinical practice, particularly in the form of collagen-based patches, films, and sponges derived from bovine sources. However, such collagen carries disadvantages, including the risk of disease transmission and potential viral contamination. Therefore, collagen from marine invertebrates is being actively investigated for potential clinical applications. The objective of the study is to evaluate the wound-healing potential of collagen from the biomass of the jellyfish (*Aurelia aurita*). In this study, two types of collagen sponges—one made from acid-soluble collagen modified with sodium alginate, and the other from collagen additionally cross-linked with glutaraldehyde (insoluble)—were evaluated for their wound-healing and immunostimulatory properties in a rat skin wound model. Both formulations demonstrated wound-healing and antifibrotic effects, as well as improved the clinical welfare of animals. The insoluble formulation demonstrated the strongest regenerative effect during the early stage of skin wound healing (day 1), outperforming both the soluble formulation and the negative control. However, only the soluble formulation exhibited anti-inflammatory activity. The insoluble formulation improved postoperative welfare in rats, as evidenced by reduced weight loss and a higher behavioral welfare index relative to the untreated control group. In contrast, the immunostimulatory and epithelialization-accelerating effects of the soluble formulation were weaker than those of the insoluble formulation. Moreover, the soluble sponge exhibited limited granulation tissue vascularization, indicating potential adverse effects during therapeutic application. This work highlights the wound-healing and immunostimulatory potential of collagen sponges derived from *A. aurita* and supports their further investigation in diverse wound models and subsequent clinical studies.

Keywords:
Acid-soluble collagen; *Aurelia aurita*; Collagen matrix; Histological signs; Inflammatory markers; Skin wound defect

***Corresponding author:**
Yuliya Kulikova,
ivkulikova@kantiana.ru

How to cite this article:
Kulikova Y, Popov V, Sukhikh S, *et al. In vivo* evaluation of marine collagen sponge for wound healing in a rat model. *Biomater Transl.* 2025

doi: 10.12336/bmt.25.00075

1. Introduction

Skin wounds are a common result of trauma, burns, infections, genetic abnormalities, and other diseases.[1,2] The treatment of skin damage aims to restore tissue integrity through processes such as inflammation, cell division, differentiation, and vascularization.[3] Proper wound healing can be achieved through the re-epithelialization of the epidermis and the formation of granulation tissue in the dermis. The primary factors in skin regeneration are keratinocyte migration during re-epithelialization and the infiltration of fibrogenic and angiogenic cells into granulation tissue.[4-6] At present, new therapeutic approaches are being explored to promote proper re-epithelialization, including the use of natural materials.[6]

Certain biomaterials, such as collagen, are effective in wound healing because they protect wounds from infection and help maintain appropriate moisture levels. When used together with antibiotics, these materials contribute to the overall improvement of patient health.[7] Collagen, a widely distributed natural protein, has long been applied in wound treatment as a dressing material in various forms, including

bandages, powders, and gels.[8] Structurally, collagen is a large protein molecule consisting of three polypeptide alpha chains. Upon enzymatic hydrolysis, it produces low-molecular-weight bioactive peptides with a wide range of biological functions.[9] In the skin, collagen peptides act as pseudo-degradation products, sending false signals to fibroblasts to synthesize new collagen fibers. In addition, collagen peptides exhibit chemotactic properties, stimulating cell migration and proliferation, both of which are critical processes in wound healing.[10]

Modern regenerative medicine extensively uses collagen-based products, most commonly derived from terrestrial animals such as cattle and pigs.[11] However, such sources pose several disadvantages, including the risk of transmitting various diseases (such as spongiform encephalopathy) and potential viral contamination.[12] For this reason, there is a constant need to identify alternative sources of collagen. Marine organisms, including fish, starfish, sponges, and jellyfish, are a promising resource for collagen extraction, offering metabolic compatibility and eliminating the risk of contamination by animal pathogens.[3,13]

Studies have reported that marine collagen derived from fish, jellyfish, and sponges can accelerate wound healing.[14-19] These effects are primarily mediated by enhanced fibroblast and keratinocyte migration, increased vascularization, and promotion of epidermal growth.[20,21]

Jellyfish, in particular, have gained attention as a high-quality marine source of collagen and its hydrolysates for tissue engineering and regenerative medicine, owing to their unique physicochemical and functional properties as well as their accessibility.[22] Collagen hydrolysates from jellyfish have demonstrated antioxidant, anti-aging, anticoagulant, and immunoregulatory activities.[23-25] In addition, collagen matrices obtained from *Cassiopea andromeda*, *Rhopilema esculentum*, *Cotylorhiza tuberculata*, *Pelagia noctiluca*, and *Rhizostoma pulmo* have been shown to accelerate wound healing.[7,26-29] However, there is limited research on the potential use of *Aurelia aurita* collagen as a substrate for tissue engineering.[30,31]

We have previously isolated acid-soluble type I collagen (molecular weight: 100–115 kDa) from *A. aurita*, native to the Baltic Sea. This collagen was not cytotoxic to primary human fibroblasts. *In vitro* wound healing assays using fibroblasts and HaCaT keratinocytes showed regenerative potential, with a 24.5% increase in wound healing rate,[32] indicating its prospects for use in regenerative medicine.

This study aimed to evaluate the wound-healing efficacy and immunostimulatory activity of two types of collagen sponge matrices derived from *A. aurita*—the most common jellyfish species in the Baltic Sea—using a rat skin wound model. Specifically, the study investigated an insoluble form cross-linked with glutaraldehyde and a soluble form modified with sodium alginate and reported their wound-healing, antifibrotic, and immunomodulatory activities.

2. Methods

2.1. Collagen samples derived from *A. aurita*

The study investigated two types of collagen substrate (acid-soluble collagen) obtained from the Baltic Sea jellyfish (*A. aurita*): (i) Sample 1: An insoluble form, cross-linked with glutaraldehyde, presented as a pale-yellow dry sponge with a diameter of 20 mm and (ii) Sample 2: A soluble form, modified with sodium alginate, also presented as a pale-yellow dry sponge with a diameter of 20 mm.

Collagen was obtained using the previously described method.[32,33] Extraction was performed for 3 days at 4°C in 0.5 M acetic acid. Acid-soluble collagen was precipitated by adding NaCl (52.6 g/L), and the precipitate was dissolved in two volumes of 0.5 M acetic acid. The resulting solution was dialyzed at 4°C: first for 72 h against 0.1 M acetic acid and then for 72 h against distilled water. Before application in animals, the collagen samples were gamma-sterilized with a dose of 15.0 ± 0.5 kGy before using the GU-200M gamma unit based at Joint-Stock Company Scientific Research Institute of Technical Physics and Automation, Moscow, Russia.

2.2. *In vivo* experiments

2.2.1. Animal model

All animal studies were approved by the Bioethics Commission of the M.V. Lomonosov Moscow State University (protocol No. IR.IUMS.REC.1398.962). Standardized housing conditions were maintained for experimental animals: placement in standard polycarbonate cages on open stainless-steel racks (two rats per cage), air temperature of 18–26°C, air humidity of 46–65%, air exchange rate of 10–15 room volumes per hour, light cycle of 12-h darkness/12-h light, with access to feed (in accordance with GOST 34566–2019) and water *ad libitum*. A total of 20 healthy female Wistar rats (specific-pathogen-free category, 5 months old, 272–384 g, obtained from the nursery of the Institute of Cytology and Genetics SB RAS, Moscow, Russia), who were not in breeding, were randomized into four groups: two treatment groups, a negative control group, and a positive control group (**Table 1**). As a control treatment, a 10% methyluracil ointment (Tula Pharmaceutical Factory, LLC, Russia) was applied externally. The experiment was conducted over 25 days, with the manipulation schedule as shown in **Table 2**.

2.2.2. Measurement of animal body weight

The weighing of the animals was carried out using the Vibra AJ-1200CE electronic scale (Shinko Denshi, Japan). The maximum weighing limit of the scale is 1,200 g, the minimum weighing limit is 0.5 g, and the error is ±0.01 g. Weighing was

[1]Higher School of Living Systems, Institute of Medicine and Life Sciences, Immanuel Kant Baltic Federal University, Kaliningrad, Kaliningrad Oblast, Russia; [2]Research Laboratory of Translational Medicine, Faculty of Medicine, Lomonosov Moscow State University, Moscow, Russia; [3]Department of Translational Medicine Research Institute, Faculty of Medicine, Lomonosov Moscow State University, Moscow, Russia

Table 1. Experimental animal grouping

Group number	Number of animals	Wound type	Treatment
Group 1	5	Wound on the skin	Collagen sponge Sample 1
Group 2	5	Wound on the skin	Collagen sponge Sample 2
Group 3 (negative control)	5	Wound on the skin	-
Group 4 (positive control)	5	Wound on the skin	Methyluracil ointment
Total	20		

Table 2. Timeline of experimental procedures

Day	Procedures
1–7	Acceptance and quarantine of animals, handling.
8	Animal labeling, blood sampling, and weighing.
11	Surgery for the formation of a wound defect on the skin, wound area measurement, and initiation of treatment.
11–25	Daily inspection and assessment of animal welfare.
12 (1st p.d.)	Wound area measurement, wound dressing.
14 (3rd p.d.)	Weighing, wound area measurement.
18 (7th p.d.)	Weighing, wound area measurement, and blood sampling.
21 (10th p.d.)	Weighing, wound area measurement.
25 (14th p.d.)	Blood sampling, euthanasia, wound area measurement, and collection of a skin flap with the wound defect for histological analysis.

Abbreviation: p.d.: Postoperative day

carried out according to the manipulation schedule at the same time of each day to avoid diurnal fluctuations in body weight.

2.2.3. Induction of a standard skin wound

The surgical area was prepared by shaving the interscapular area and disinfecting the skin with 70% ethanol. Under isoflurane anesthesia, a circular full-thickness skin defect (2 cm in diameter, extending to the subcutaneous muscle of the trunk) was created by excising a skin flap with pointed scissors using a template. According to the experimental group, the wound surface was treated with one of the following: Sample 1, Sample 2, a dry sterile gauze cloth, or a gauze swab with methyluracil ointment. All wounds were then covered with a gauze cloth and secured with a self-closing bandage.

Anesthesia was induced in a chamber and maintained with a face mask using an inhaled mixture of 2–4% isoflurane (Laboratorios Karizoo, Spain) in approximately 93% oxygen, delivered through a V3000 Parkland Scientific evaporator connected to the Nuvo Lite 52 oxygen concentrator (Parkland Corporation, Canada). For perioperative analgesia, meloxicam was administered subcutaneously at a dose of 3 mg/kg before surgery.

2.2.4. Application of collagen sponges to the wound surface

Under general anesthesia, a skin wound with a diameter of 20 mm was created. In experimental animals, the wound defect was closed with a test collagen sponge sample (Sample 1 or Sample 2) for 7 days and covered with an aseptic dressing. The bandage was removed on postoperative day 7.

2.2.5. Measurement of the wound surface area

On the day of surgery and on postoperative days 1, 3, 7, 10, and 14, the wound size was assessed by measuring two perpendicular diameters with a ruler and photographing the wound in direct projection with a ruler included for scale using the FZ55 digital camera (Eastman Kodak Company, United States [US]). Subsequently, images were analyzed using the ImageJ software (https://imagej.net/ij/): calibration was performed according to the ruler in each image, and the wound margins were outlined to calculate the wound area. A comparison of wound diameter measurements obtained from three animals using both the ruler and the ImageJ program showed no significant differences; therefore, all subsequent calculations were performed using the software method.

2.2.6. Assessment of animal welfare

Throughout the entire postoperative period, animals were examined daily, and their welfare was assessed according to the following criteria: animal appearance, activity, and facial signs of pain. Activity and appearance were scored on a 0–2 scale, where 0 indicated normal condition, 1 indicated minor deviations, and 2 indicated considerable deviations. The facial signs of pain were evaluated in accordance with previous studies,[34] including narrowing of the eyes, wrinkling of the nose, pulling the whiskers back, and putting the ears back, with each feature assigned 1 point. Higher scores indicate poorer conditions, with the maximum score being 8.

2.2.7. Measurement of inflammatory markers in the blood

To measure the markers of inflammation in the blood, 0.5–0.7 mL of blood was collected from the sublingual vein under isoflurane anesthesia. Samples were placed in 2-mL Eppendorf tubes and centrifuged at 5,000 × g for 15 min using an Eppendorf Centrifuge 5415 R (Eppendorf, Germany). The separated serum was transferred into sterile tubes labeled with animal number and sampling date and stored in a Haier freezer (Haier, China) at −80°C until analysis.

After collecting all the samples, they were transported for analysis in a thermally insulated container with cooling elements to prevent thawing. The parameters of lipid metabolism were evaluated as presented in **Table 3**.

2.2.8. Collection of materials for histological analysis

On postoperative day 14, animals were euthanized using carbon dioxide. A skin flap containing the wound defect and 0.5–1.0 cm of surrounding healthy tissue was excised and fixed in 10% neutral buffered formalin (Biovitrum, Russia). The samples were then processed for histological and immunohistochemical studies.

2.2.9. Histological analysis and immunohistochemistry

Skin flaps were fixed for at least 48 h in 10% buffered formalin at a material-to-fixative ratio of 1:20. After fixation, tissue fragments were trimmed and placed in labeled histology cassettes. Samples were processed in an automatic vacuum

Table 3. Target inflammatory markers and their reagent kits

Markers	Reagents
Interleukin 6 (IL)-6	Rat IL-6 ELISA Kit (catalog no.: RK00020, ABclonal, China)
IL-10	Rat IL-10 ELISA Kit (catalog no.: RK00050, ABclonal, China)
Tumor necrosis factor (TNF-α)	Rat TNF-α ELISA Kit (catalog no.: A133Ra, Cloud-Clone Corp., China)

Abbreviation: ELISA: Enzyme-linked immunosorbent assay.

processor (ASP300 S, Leica Biosystems, Germany) using seven changes of isopropyl alcohol (Komponent-Reaktiv, Russia) for 45 min each, followed by three changes of paraffin (Biovitrum, Sweden) for 60 min at 60°C. Embedding was performed in reusable metal molds using the Leica HistoCore Arcadia embedding station (Leica Biosystems, Germany).

Paraffin blocks were sectioned at 4 μm on the RM 2125 RTS manual rotary microtome (Leica Biosystems, Germany). Sections were floated on the Slidebanya-30/60 water bath (Technom KB, Russia) for flattening and mounted on PCI adhesive-coated slides (Biovitrum, Sweden).

For histology, the dewaxing, discoloration, and brightening of sections were performed in the automatic stainer ST5010 AXL (Leica Biosystems, Germany). Staining was performed with hematoxylin and eosin and van Gieson's method using Biovitrum reagents, following the manufacturer's instructions. Stained sections were manually coverslipped using the Consul-Mount mounting medium (Thermo Fisher Scientific, US).

For immunohistochemistry, the dewaxing of sections was carried out using a standard protocol, with three changes of xylene for 10 min each, three changes of ethanol for 5 min each, and a final wash in distilled water. Antigen retrieval was carried out by heating in tromethamine-ethylenediaminetetraacetic acid buffer (pH = 9.1; for fibroblast growth factor 1 and epidermal growth factor [EGF]) or citrate buffer (pH = 6; for cluster of differentiation 31) at 95–98°C for 30 min. Primary antibodies (1:100) were applied overnight at 4°C in a humid chamber, followed by phosphate-buffered saline (pH 7.2–7.4) washes with three changes of 5 min each. Secondary antibodies (1:200) were applied overnight at 4°C under the same conditions. Immune complexes were visualized using the Histofine DAB-3S Peroxidase Chromogen/Substrate kit (Nichirei Biosciences Inc., Japan). Slides were mounted with the Consul-Mount mounting medium and examined under the ADF E300 research microscope (ADF, China). Histological processing and descriptions were carried out by an operator blinded to sample identity to minimize subjectivity in the analysis, using ImageJ. The list of assessed markers is presented in **Table 4**.

2.2.10. Statistical analysis

Descriptive statistics were applied to all data. Normality of distribution was assessed using the Kolmogorov-Smirnov test. For normally distributed data, the mean (M) and standard deviation (SD) were calculated and presented as M ± SD, together with the sample size (n). For non-normally distributed data, the median (Me) and interquartile range (Q1–Q3) were reported. Intergroup differences were analyzed using parametric or nonparametric methods, depending on data distribution. Normally distributed data were evaluated with one-way analysis of variance (ANOVA) (using 30.0.0 Statistical Package for the Social Sciences Statistics, International Business Machines Corporation, US) and Student's t-test. Non-normally distributed data were evaluated with the Kruskal–Wallis test with *post hoc* pairwise rank comparisons and the Mann–Whitney U test. The non-parametric Wilcoxon matched-pairs test was used to compare consecutive measurements within groups. Statistical analyses, except the one-way ANOVA test, were performed using Statistica (13.3.721, StatSoft Inc., US). A $p<0.05$ was considered statistically significant.

Table 4. Assessed markers of regenerative processes and reagent kits

Parameter	Reagents
EGF	100 mg Polyclonal antibody to EGF (rat) (PAA560Ra01, Cloud-Clone Corp., China)
FGF1	100 mg Polyclonal antibody to FGF1 (rat) (PAA032Ra01, Cloud-Clone Corp., China)
CD31	100 mg Polyclonal antibody to PECAM1 (rat) (PAA363Ra01, Cloud-Clone Corp., China)
AT for visualization	1 mL HRP-labeled antibody goat-anti-rabbit IgG (H+L) (S0001, Cloud-Clone Corp., China)

Abbreviations: AT: Goat anti-rabbit immunoglobulin G; CD31: Cluster of differentiation 31; EGF: Epidermal growth factor; FGF1: Fibroblast growth factor 1; HRP: Horseradish peroxidase; PECAM1: Platelet endothelial cell adhesion molecule.

3. Results

3.1. Body weight

Since body weight is one of the main integral biomedical variables describing animal welfare, the dynamics of rat body weight were monitored over the 14 days following skin defect induction, with baseline values taken before surgery. The final measurement was recorded before euthanasia. The comparison results are shown in **Figure 1**.

The analysis of body weight dynamics showed that, except for the negative control group, all groups experienced a significant decrease in body weight by postoperative day 14 (Wilcoxon matched-pairs test, $p<0.05$). The rats treated with Sample 2 showed the most significant weight loss, with an average of 11%. In the Sample 1-treated group, there was a tendency for weight gain following initial weight loss after postoperative day 7.

3.2. Clinical signs of animals

The clinical signs of rat well-being were assessed from postoperative day 1 to day 9, as by day 9, almost all animals ceased to show signs of distress. The cumulative scores reflecting animal distress (higher scores indicating greater distress) are shown in **Figure 2**.

In all groups, by postoperative day 9, the condition of the animals had improved significantly (Wilcoxon matched-pairs test, $p<0.05$). The daily dynamics of improvement were similar across groups; however, in the negative control group, improvement plateaued after postoperative day 6, whereas it

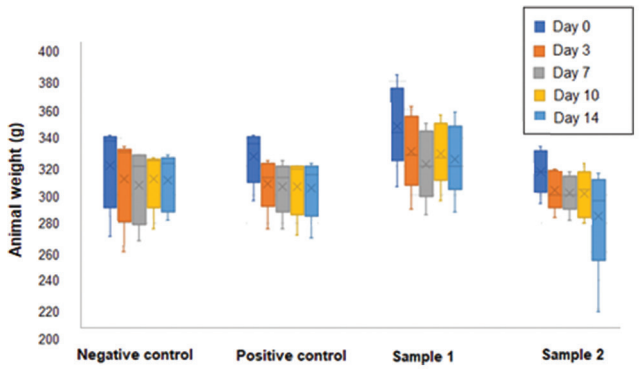

Figure 1. Body weight dynamics across experimental groups. Notes: Data are presented as M ± standard deviation; Day indicates postoperative day.

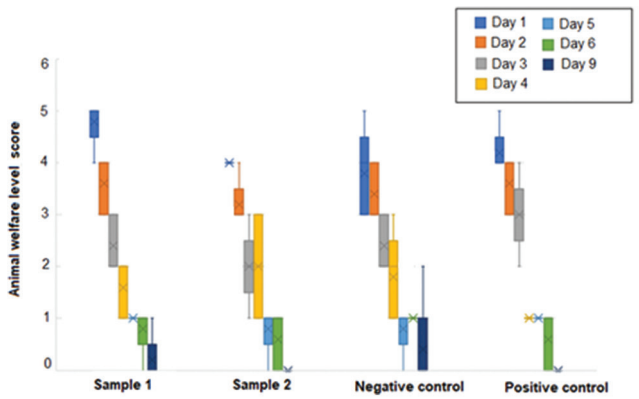

Figure 2. Dynamics of the integral score of distress across experimental groups
Notes: Data are presented as M ± standard deviation; Day indicates postoperative day

continued in all other groups. The final distress score in the negative control group was higher (at a trend level) compared with the other groups, while in the groups treated with Sample 1 or Sample 2, it did not differ from the positive control.

3.3. Wound surface area

Experimental samples and the reference drug, methyluracil ointment, were applied to the wound surfaces immediately after the operation. The wounds in both experimental and control groups were then covered with self-tightening bandages to retain the drug and prevent contamination. To measure the wound surfaces in anesthetized rats, the dressings were replaced as needed. Representative photographs of the wound surfaces from different experimental groups are shown in **Figure 3**. These images demonstrate that the experimental collagen sponges formed a layer on the wound surfaces, which mixed with wound discharge and promoted the formation of a fragmentary scab. On postoperative day 7, the bandages (along with residual collagen sponge materials) were removed, and thereafter, the wound surfaces remained open.

Table 5 shows the mean wound surface area in animals. To assess the dynamics of wound reduction across groups, relative changes were calculated with reference to the wound surface area measured immediately after surgery. These data are shown in **Figure 4**.

Table 5. Changes in wound surface area across experimental groups

Postoperative day	Wound surface area (cm²)			
	Sample 1	Sample 2	Negative control	Positive control
Day 0	321.59±31.27	305.83±26.76	308.85±12.56	312.96±24.21
Day 1	279.26±41.12	309.22±26.65	335.36±58.50	310.25±41.48
Day 3	271.09±29.82	273.62±20.81	303.23±40.71	304.54±66.48
Day 7	204.26±20.94	190.15±14.03	150.74±32.83	201.71±11.5
Day 10	94.40±26.99	81.33±31.68	94.98±40.03	70.91±48.96
Day 14	26.06±5.90	23.06±8.42	34.86±17.33	19.57±13.43

Animals in all groups showed similar dynamics of wound surface changes: from postoperative day 1 to day 3, the wound area decreased slightly, followed by accelerated healing, partly attributed to the removal of bandages on day 7. From postoperative day 10 to day 14, the reduction in wound size was insignificant. By postoperative day 14, the skin defect in any rat did not exceed 15% of the original area, consistent with previously reported dynamics of skin wound healing in rats.[35]

3.4. Systemic inflammatory markers

To assess the dynamics of systemic inflammatory markers, concentrations of interleukin (IL)-6, IL-10, and tumor necrosis factor-alpha (TNF-α) in blood plasma were measured at 2 time points: before wound induction and immediately before euthanasia on postoperative day 14. The levels of IL-6 were undetectable in all animals across all groups in both time points, despite the kit standards performing as expected. This potentially reflects the known dynamics of IL-6 in rat skin wound models, where basal levels are very low, increase rapidly after injury, and decrease after 48 h.[36,37] Therefore, cytokine concentrations at the selected time points were probably below the detection limit. The measured concentrations of IL-10 and TNF-α are shown in **Figure 5**.

A comparison of IL-10 concentrations in rat blood plasma at baseline and after euthanasia is shown in **Figure 5A**. A significant increase from baseline to endpoint was recorded only in the Sample 2-treated group (Wilcoxon matched-pairs test, $p<0.05$). No significant differences were found in other groups.

3.5. Histological and immunohistochemical analyses

For histological analysis, three tissue fragments were selected for each animal, including two from opposite edges of the healed defect. Representative photomicrographs (magnification ×300) are shown in **Figure 6**.

To quantify histological signs for each animal, the following parameters were evaluated across all three fragments:

(i) Degree of epithelialization: 1 = marginal, 2 = complete without keratinized layer, and 3 = complete with keratinized layer;

(ii) Scab resolution: Complete or incomplete rejection with tissue detritus;

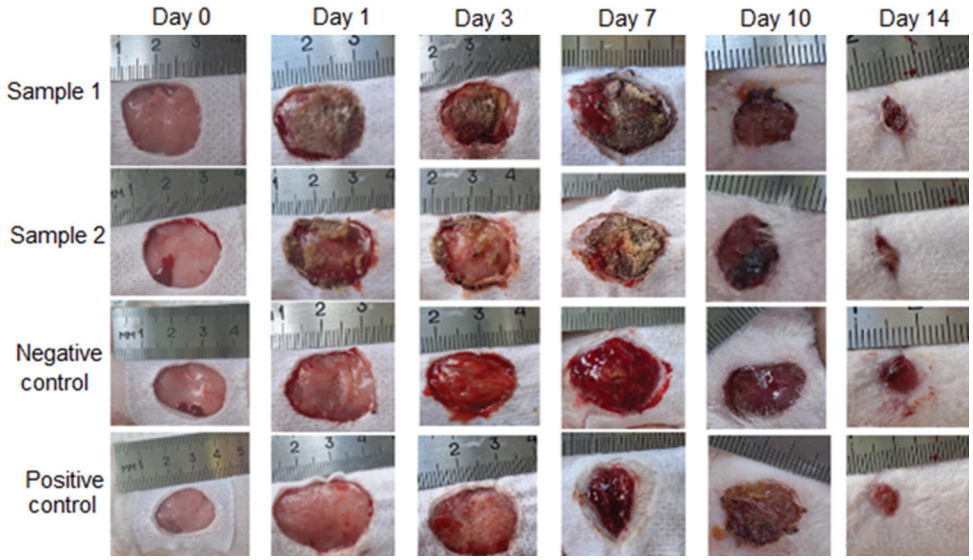

Figure 3. Representative photographs of the wound surfaces across experimental groups. In the Sample 1-treated and Sample 2-treated groups, the formation of a partial scab is noticeable.
Note: Day indicates postoperative day.

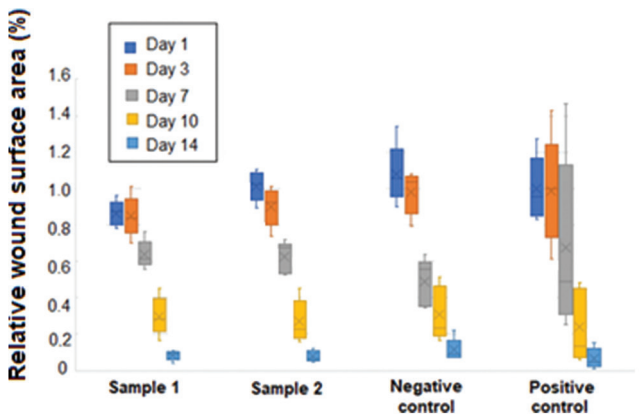

Figure 4. Relative wound surface area as a percentage of the defect area immediately after surgery across experimental groups
Notes: Data are presented as M ± standard deviation; Day indicates postoperative day.

(iii) Immune infiltration: Presence or absence in the wound area and/or granulation tissue;
(iv) Granulation tissue maturity: Immature or mature with signs of neoangiogenesis;
(v) Fibroblast migration: Presence or absence in the defect area.

Experimental groups were compared according to all the described histological features (**Figure 7**).

Figure 8 shows the results of immunohistochemical staining for markers of regenerating tissues. The markers exhibited specific staining to varying degrees. Sections were considered successfully stained when clear, marker-specific coloration was observed in the appropriate cell types (for example, endothelial cells for CD31). The proportion of animals displaying successful staining for selected markers was estimated in each group.

The endotheliocyte marker CD31 showed specific coloration in 60% of animals in the Sample 1-treated, Sample 2-treated, and negative control groups, and was not detected in any animals from the positive control group. This result is inconsistent with the low degree of granulation tissue maturation observed in the Sample 2-treated group.

Meanwhile, EGF showed the highest frequency of specific coloration in the Sample 2-treated and negative control groups, consistent with the histological data, which indicated the most active epithelial proliferation in these groups.

Similarly, FGF1 exhibited the highest frequency of specific staining in the positive and negative control groups, consistent with the observed higher frequency of fibroblast migration to the wound defect area in these groups.

In the Sample 1-treated group, the wound site showed the highest level of epithelial development and the lowest level of EGF staining, potentially reflecting the completion of re-epithelialization. Fibroblast migration to the wound area was minimal, corresponding to low FGF1 expression. At the same time, immune infiltration was more pronounced than in the negative control group, and granulation tissue was relatively mature, as confirmed by CD31 expression.

In the Sample 2-treated group, both epithelialization and fibroblast migration were intermediate between the Sample 1-treated group and the negative control. Immune infiltration was also higher compared with the negative control. The unexpectedly low level of granulation tissue maturity in this group needs further research.

4. Discussion

4.1. Animal body weight

Analysis of animal weight dynamics (**Figure 1**) showed that all groups experienced a gradual weight loss after surgery, which plateaued after postoperative day 7. Notably, weight dynamics in the Sample 1-treated group differed from the control groups: while body weight in the control groups decreased steadily, in the Sample 1-treated group, it decreased during the 1st week

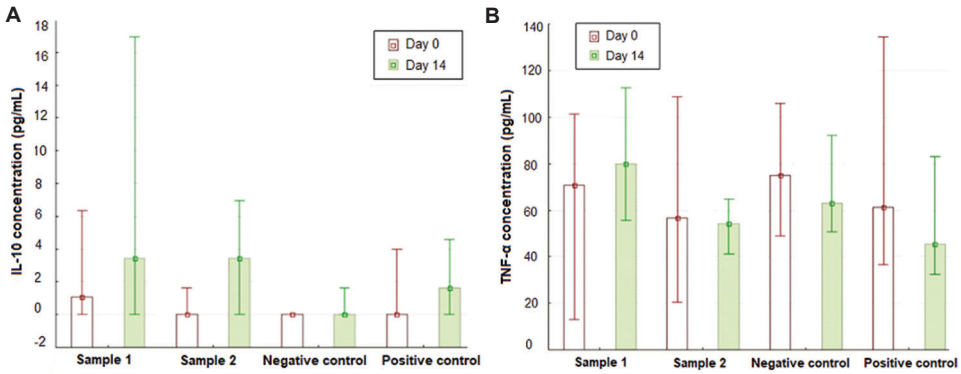

Figure 5. Changes of (A) interleukin-10 and (B) tumor necrosis factor-alpha concentrations in the blood plasma of rats across experimental groups
Notes: Data are presented as M ± standard deviation; Day indicates postoperative day.

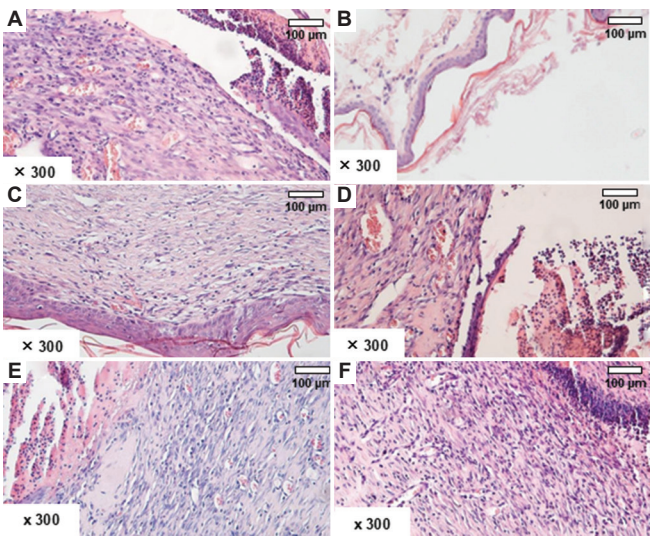

Figure 6. Histological signs used in the quantitative analysis of wound healing across experimental groups. (A) Marginal epithelialization. (B) Complete closure of the defect. (C) Complete closure of the defect by multilayer keratinizing epithelium. (D) An incompletely rejected defect is closed by fibrin deposits. (E) An incompletely rejected defect is closed by fibrin deposits. (F) Mature granulation tissue with signs of neoangiogenesis. Scale bars: 100 μm; magnifications: ×300.

but began to increase after postoperative day 7, suggesting faster recovery in this group. In contrast, the Sample 2-treated group showed no positive effect on overall animal welfare, as indicated by the weight change dynamics.

4.2. Clinical signs of animals

The dynamics of clinical signs of animal distress (**Figure 2**) showed that the highest distress levels during the first 3 postoperative days were observed in the Sample 1-treated group and the negative control. The elevated distress score on postoperative day 1 in the Sample 1-treated group was potentially due to individual variability among the animals, as differences with other groups had leveled by day 2 and thereafter. The integral scores in the experimental groups did not differ from the positive control, while the final scores were slightly lower (trend level) than in the negative control. These results further confirm that the use of collagen sponges does not lead to significant relief of animal distress.

4.3. Wound surface area

Differences in the relative reduction of wound defect area among groups were generally not significant, with the exception of the Sample 1-treated group, which showed a significantly greater reduction compared to the Sample 2-treated group and the negative control. The difference with the positive control did not reach statistical significance, potentially due to high inter-individual variability. This indicates a potential regenerative effect of Sample 1 during the early stages of skin wound healing.

During the 1st week, the Sample 1-treated and Sample 2-treated groups exhibited a smaller reduction in wound surface area, although they approached the levels seen in the control groups by postoperative day 14. One possible explanation is the mechanical closure of the wound with sponge material, which prevents effective contraction of wound edges.

Overall, the reduction of wound surfaces occurred synchronously across all groups, with residual defects ranging from 1% to 15% of the initial area by the end of the experiment. Significant acceleration of wound surface reduction in the Sample 1-treated group was observed as early as postoperative day 1.

4.4. Systemic inflammatory markers

The dynamics of systemic inflammatory markers (IL-6, IL-10, and TNF-α) in blood plasma were assessed before wound induction and on postoperative day 14 (**Figure 5**). IL-10 levels on postoperative day 14 showed a downward trend, suggesting that in the Sample 2-treated group, the inflammatory reaction was more prolonged compared to the control, reflecting a smoother course of inflammation.

Pairwise comparisons between groups at the endpoint revealed no significant differences.

A comparison of TNF-α concentrations across experimental groups showed that, except for the Sample 1-treated group, concentrations of this pro-inflammatory cytokine slightly decreased by the endpoint of the experiment compared to baseline. The opposite trend in the Sample 1-treated group may reflect a more robust inflammatory response to injury. The relationship between residual wound surface area and TNF-α

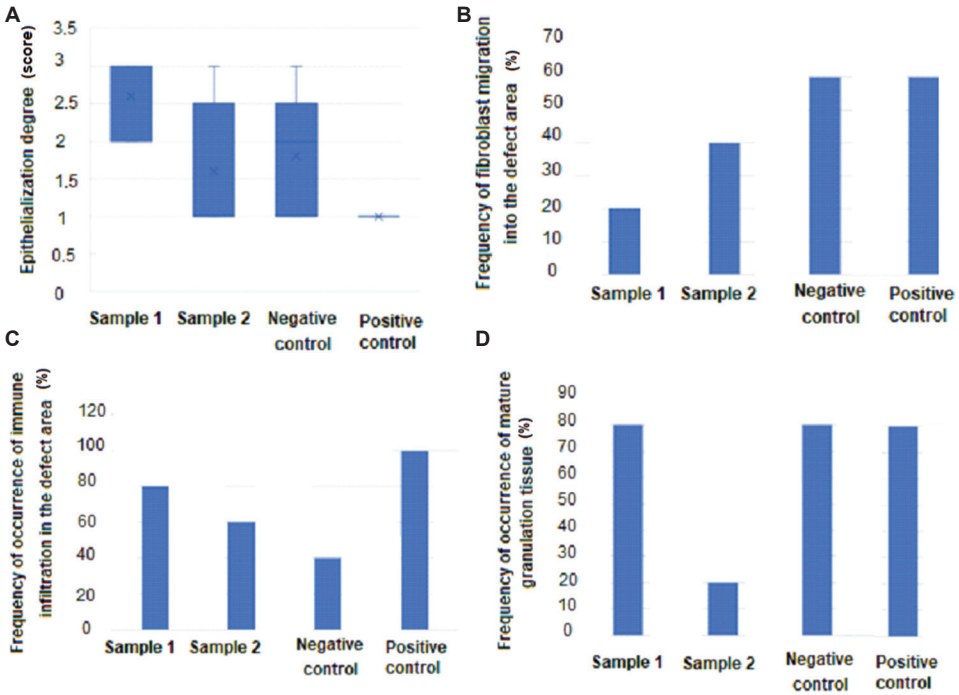

Figure 7. Comparison of quantitative histological features across experimental groups. (A) The degree of epithelialization (average score in the group). (B) The frequency of fibroblast migration to the defect area. (C) The frequency of immune infiltration in the defect area. (D) The frequency of mature granulation tissue.

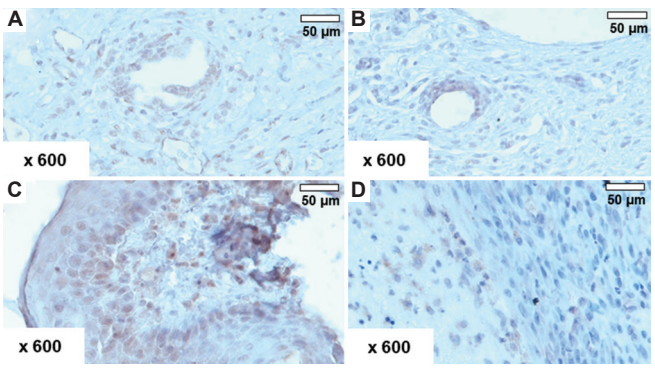

Figure 8. Immunohistochemical staining of regenerating tissue markers. (A and B) Cluster of differentiation 31, a marker of angiogenesis, is specifically stained in vascular endothelial cells formed in granulation tissue. Scale bars: 50 µm; magnifications: ×600. (C) Epithelial growth factor is expressed at the edge of the wound defect, areas where re-epithelialization begins. Scale bar: 50 µm; magnification: ×600. (D) Fibroblast growth factor is detected in some cells within the granulation tissue. Scale bar: 50 µm; magnification: ×600.

concentration at postoperative day 14 was evaluated (**Figure 9**). Plasma TNF-α levels reflect the degree of systemic inflammation. In most groups, an inverse relationship was observed: higher TNF-α concentrations were associated with smaller residual wound areas. Interestingly, in the Sample 2-treated group, the inflammatory peak occurs more gradually, and the effectiveness of wound healing did not correlate with TNF-α levels, indicating a potential anti-inflammatory effect of Sample 2.

4.5. Histological and immunohistochemical analyses

Of the 20 animals, by the end of the experiment (postoperative day 14), complete scab rejection without residue was observed in only two animals—one from the Sample 1-treated group and one from the Sample 2-treated group—indicating an effect of the tested collagen matrices. In all other cases, the wound surface was covered with fibrin deposits and tissue debris, variably infiltrated by immune cells.

Epithelialization, culminating in the formation of a multilayered keratinizing epithelium, is considered a hallmark of successful skin regeneration. Comparison of groups by averaging epithelialization scores (**Figure 7A**) showed that both experimental groups (especially in the Sample 1-treated group) demonstrated more successful epithelial formation than the controls, especially the positive control treated with methyluracil ointment. At the same time, one animal from the Sample 2-treated group showed signs of the remodeling of skin glands and hair follicles, further supporting the regenerative potential of the tested collagen matrices, particularly Sample 1.

The migration of fibroblasts into the injury zone precedes differentiation into myofibroblasts and the formation of fibrosis tissue. Thus, the low frequency of fibroblast migration in the experimental groups (**Figure 7B**), especially in the Sample 1-treated group, indicates the antifibrotic activity of the collagen samples.

In terms of the frequency of immune infiltration in the wound surface area (**Figure 7C**), both experimental groups displayed intermediate levels between the negative and positive controls, indicating an immunostimulatory effect of the collagen sponges, although less pronounced than that of methyluracil.

The maturity of the granulation tissue, primarily assessed by neovascularization, indicates the rate of regenerative

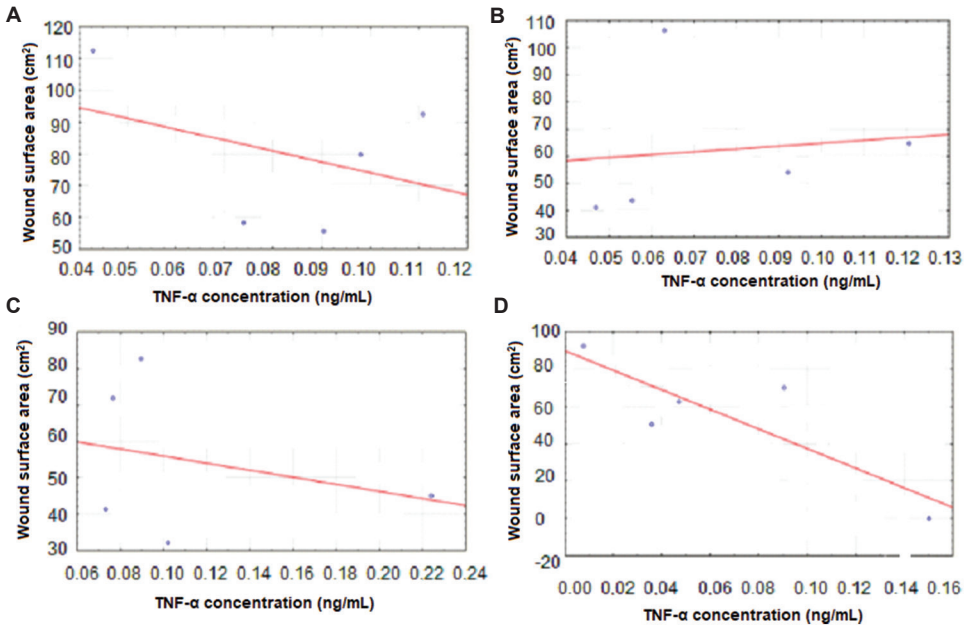

Figure 9. Relationship between wound surface area reduction and tumor necrosis factor-α concentration in blood plasma at the endpoint across experimental groups. (A) Sample 1-treated group. (B) Sample 2-treated group. (C) Negative control. (D) Positive control.

processes in the wound surface area. Most groups showed high granulation tissue maturity, with the exception of the Sample 2-treated group, in which mature granulation tissue was found in only one of five rats. This result should be taken into account in the further development of drugs based on Sample 2, as it may indicate potential side effects.

5. Conclusions

The present study demonstrates the wound-healing and immunostimulatory potential of two collagen matrix formulations (soluble and insoluble in water and biological media) obtained from *A. aurita*, following a single application to the wound surface in a rat skin wound model. The insoluble formulation, modified with glutaraldehyde, showed a tendency to reduce postoperative weight loss and improved overall clinical welfare compared to the negative control. It also produced the greatest reduction in wound surface during postoperative day 1. Histological studies revealed accelerated epithelialization, antifibrotic activities, and immunostimulatory effects, although no anti-inflammatory effect was detected. The soluble collagen formulation, modified with sodium alginate, also improved the final clinical condition of the animals compared to the negative control and showed anti-inflammatory activity. Histologically, it demonstrated immunostimulatory effects and enhanced epithelialization, although to a lesser degree than the insoluble formulation. A low degree of granulation tissue vascularization was observed with the soluble formulation, indicating potential side effects during its therapeutic use. Therefore, further studies are needed across a wide range of wound models to clarify the biological activity of collagen matrices derived from *A. aurita* and to identify potential side effects before clinical studies.

Acknowledgement
None.

Financial support
The work was supported by the Ministry of Science and Higher Education of the Russian Federation, contract no. 075-15-2023-601 (ext. No. 13.2251.21.0219).

Conflicts of interest statement
The authors declare they have no competing interests.

Author contributions
Conceptualization: OB and VP; *Funding acquisition*: OB; *Investigation*: YK, VP, AS, and MD; *Methodology*: VP; *Project administration*: OB; *Resources*: OB; *Visualization:* LD; *Writing—original draft*: YK and SS; *Writing—review & editing:* OB and YK. All authors have read and agreed to the published version of the manuscript.

Ethics approval and consent to participate
All animal studies were approved by the Bioethics Commission of the M.V. Lomonosov Moscow State University (protocol No. IR.IUMS.REC.1398.962).

Consent for publication
Not applicable.

Availability of data
The authors confirm that the data supporting the findings of this study are available within the article. Raw data that support the findings of this study are available from the corresponding author upon reasonable request.

References

1. Harder J, Schröder JM, Gläser R. The skin surface as antimicrobial barrier: Present concepts and future outlooks. *Exp. Dermatol.* 2013;22:1-5. doi: 10.1111/exd.12046
2. Hall AH, Mathieu L, Maibach HI. Acute chemical skin injuries in the United States: A review. *Crit Rev Toxicol.* 2018;48:540-554. doi: 10.1080/10408444.2018.1493085
3. Geahchan S, Baharlouei P, Rahman A. Marine collagen: A promising biomaterial for wound healing, skin anti-aging, and bone regenera. *Mar Drugs.* 2022;20:61. doi: 10.3390/md20010061
4. Gurtner GC, Werner S, Barrandon Y, Longaker MT. Wound repair and

regeneration. *Nature.* 2008;453:314-321.
doi: 10.1038/nature07039

5. Martin P. Wound healing-aiming for perfect skin regeneration. *Science.* 1997;276:75-81.
doi: 10.1126/science.276.5309.75
6. Sumiyoshi H, Okamura Y, Kawaguchi AT, *et al.* External administration of moon jellyfish collagen solution accelerates physiological wound healing and improves delayed wound closure in diabetic model mice. *Regen Ther.* 2021;18:223-230.
doi: 10.1016/j.reth.2021.06.008
7. Felician FF, Yu RH, Li MZ, *et al.* The wound healing potential of collagen peptides derived from the jellyfish *Rhopilema esculentum. Chin J Traumatol.* 2019;22(1):12-20.
doi: 10.1016/j.cjtee.2018.10.004
8. Hochstein AO, Bhatia A. Collagen: Its role in wound healing. *Wound Manag.* 2014;4(1):104-109.
9. Gomez-Guillen MC, Gimenez B, Lopez-Caballero ME, Montero MP. Functional and bioactive properties of collagen and gelatin from alternative sources: A review. *Food Hydrocolloids.* 2011;25:1813-1827.
doi: 10.1016/j.foodhyd.2011.02.007
10. Banerjee P, Suguna L, Shanthi C. Wound healing activity of a collagen-derived cryptic peptide. *Amino Acids.* 2015;47:317-328.
doi: 10.1007/s00726-014-1860-6
11. Kulikova YV, Sukhikh SA, Babich OO. Marine collagen extraction methods for regenerative medicine. *Regener Org Tiss (Russ).* 2024;2(1):29-45. (In Russ).
doi: 10.60043/2949-5938-2024-1-29-45
12. Widdowson PJ, Picton JA, Vinc V, Wright CJ, Mearns-Spragg A. *In vivo* comparison of jellyfish and bovine collagen sponges as prototype medical devices. *J Biomed Mater Res B Appl Biomater.* 2018;106(4):1524-1533.
doi: 10.1002/jbm.b.33959
13. Tajbakhsh E, Khamesipour A, Hosseini SR, Kosari N, Shantiae S, Khamesipour F. The effects of medicinal herbs and marine natural products on wound healing of cutaneous leishmaniasis: A systematic review. *Microb Pathog.* 2021;161(Pt A):105235.
doi: 10.1016/j.micpath.2021.105235
14. Yamada S, Yamamoto K, Ikeda T, Yanagiguchi K, Hayashi Y. Potency of fish collagen as a scaffold for regenerative medicine. *Biomed Res. Int.* 2014;2014:302932.
doi: 10.1155/2014/302932
15. Zhou T, Wang N, Xue Y, *et al.* Electrospun tilapia collagen nanofibers accelerating wound healing via inducing keratinocytes proliferation and differentiation. *Colloids Surf B Biointerfaces.* 2016;143:415-422.
doi: 10.1016/j.colsurfb.2016.03.052
16. Sampath Kumar NS, Nazeer RA, Jaiganesh R. Wound healing properties of collagen from the bone of two marine fishes. *Int J Pept Res Ther.* 2012;18:185-192.
doi: 10.1007/s10989-012-9291-2
17. Shalaby M, Agwa M, Saeed H, Khedr SM, Morsy O, El-Demellawy MA. Fish scale collagen preparation, characterization and its application in wound healing. *J Polym Environ.* 2020;28:166-178.
doi: 10.1007/s10924-019-01594-w
18. Feng X, Zhang X, Li S, *et al.* Preparation of aminated fish scale collagen and oxidized sodium alginate hybrid hydrogel for enhanced full-thickness wound healing. *Int J Biol Macromol.* 2020;164:626-637.
doi: 10.1016/j.ijbiomac.2020.07.058
19. Pal P, Srivas PK, Dadhich P, *et al.* Accelerating full thickness wound healing using collagen sponge of Mrigal fish (*Cirrhinus cirrhosus*) scale origin. *Int J Biol Macromol.* 2016;93:1507-1518.
doi: 10.1016/j.ijbiomac.2020.07.058
20. Wang J, Xu M, Liang R, Zhao M, Zhang Z, Li Y. Oral administration of marine collagen peptides prepared from Chum Salmon (*Oncorhynchus Keta*) improves wound healing following cesarean section in rats. *Food Nutr. Res.* 2015;59:26411.
doi: 10.3402/fnr.v59.26411
21. Chen J, Gao K, Liu S, *et al.* Fish collagen surgical compress repairing characteristics on wound healing process *in vivo. Mar Drugs.* 2019;17:33.
doi: 10.3390/md17010033
22. Binlateh T, Hutamekalin P, Benjakul S, Chotphruethipong L. Antioxidant and anti-atherosclerosis activities of hydrolyzed jellyfish collagen and its conjugate with black jelly mushroom extract. *Foods.* 2024;13(15):2463.
doi: 10.3390/foods13152463
23. Chiarelli PG, Suh JH, Pegg RB, Chen J, Solval KM. The emergence of jellyfish collagen: A comprehensive review on research progress, industrial applications, and future opportunities. *Trends Food Sci Technol.* 2023;141:104206.
doi: 10.1016/j.tifs.2023.104206
24. Ahmed Z, Powell LC, Matin N, *et al.* Jellyfish collagen: A biocompatible collagen source for 3D scaffold fabrication and enhanced chondrogenicity. *Mar Drugs.* 2021;19(8):405.
doi: 10.3390/md19080405
25. Costa R, Capillo G, Albergamo A, *et al.* A multi-screening evaluation of the nutritional and nutraceutical potential of the Mediterranean jellyfish *Pelagia noctiluca. Mar Drugs.* 2019;17(3):172.
doi: 10.3390/md17030172
26. Sewing J, Klinger M, Notbohm H. Jellyfish collagen matrices conserve the chondrogenic phenotype in two- and three-dimensional collagen matrices. *J Tissue Eng Regen Med.* 2017;11(3):916-925.
doi: 10.1002/term.1993
27. D'Ambra I, Merquiol L. Jellyfish from fisheries by-catches as a sustainable source of high-value compounds with biotechnological applications. *Mar Drugs.* 2022;20(4):266.
doi: 10.3390/md20040266
28. Fernandez-Cervantes I, Rodriguez-Fuentes N, Leon-Deniz LV, *et al.* Cell-free scaffold from jellyfish *Cassiopea andromeda* (*Cnidaria*; *Scyphozoa*) for skin tissue engineering. *Mater Sci Eng C.* 2020;111:110748.
doi: 10.1016/j.msec.2020.110748
29. Addad S, Exposito JY, Faye C, Ricard-Blum S, Lethias C. Isolation, characterization and biological evaluation of jellyfish collagen for use in biomedical applications. *Mar Drugs.* 2011;9(6):967-983.
doi: 10.3390/md9060967
30. Balikci E, Baran ET, Tahmasebifar A, Yilmaz B. Characterization of collagen from jellyfish *Aurelia aurita* and investigation of biomaterials potentials. *Appl Biochem Biotechnol.* 2024;196(9):6200-6221.
doi: 10.1007/s12010-023-04848-5
31. Rachmawati R, Hidayat M, Permatasari N, Widyarti S. Jellyfish (*Aurelia aurita*) collagen scaffolds potential in alveolar bone regeneration. *F1000Res.* 2021;10:318.
doi: 10.12688/f1000research.28402.1
32. Barzkar N, Sukhikh SA, Cheliubeeva EY, *et al. Aurelia aurita* jellyfish collagen: Recovery properties. *Food Raw Mater.* 2025;13(2):296-305.
doi: 10.21603/2308-4057-2025-2-648
33. Balikci E, Baran ET, Tahmasebifar A, Yilmaz B. Characterization of collagen from jellyfish *Aurelia aurita* and *Aurelia aurita* jellyfish collagen: Recovery properties. *Food Raw Mater.* 2025;13(2):296-305.
doi: 10.21603/2308-4057-2025-2-648
34. Sotocinal SG, Sorge RE, Zaloum A, *et al.* The rat grimace scale: A partially automated method for quantifying pain in the laboratory rat via facial expressions. *Mol Pain.* 2011;7:55.
doi: 10.1186/1744-8069-7-55
35. Silina EV, Manturova NE, Artyushkova EB, *et al.* Dinamics of skin wound healing with the use of injectable regeneration stimulators in rats. *Patol Fiziol Eksp Ter.* 2020;64(3):54-63. (In Russ).
doi: 10.25557/0031-2991.2019.03.54-63
36. Alpidovskaya OV. Plasma levels of IL-6, IL-10, IL-18, TNFα under the conditions of tobacco intoxication and after treatment with aminophthalhydrazide. *Med Immunol (Russ).* 2024;26(3):613-616. (In Russ).
doi: 10.15789/1563-0625-PLO-2907
37. Surniyantoro HN, Abinawanto, Bowolaksono A, *et al.* IL-6 and IL-10 levels in rats blood plasma as immune responses post radioiodine (I-131) administration. *Asian Pac J Cancer Prev.* 2024;25(3):1017-1023.
doi: 10.31557/APJCP.2024.25.3.1017

Received: June 27, 2025
Revised: September 2, 2025
Accepted: September 11, 2025
Available online: October 23, 2025